RESEARCH ARTICLE

Urolithin A suppresses tumor progression and induces autophagy in gastric cancer via the PI3K/Akt/mTOR pathway

Yingjing Zhang[1] | Lin Jiang[1] | Pengfei Su[1] | Tian Yu[1] | Zhiqiang Ma[1] | Yuqin Liu[2] | Jianchun Yu[1] ⬤

[1]Department of General Surgery, Peking Union Medical College Hospital, Chinese Academy of Medical Sciences and Peking Union Medical College, Beijing, China

[2]Department of Pathology, Institute of Basic Medical Sciences, Chinese Academy of Medical Sciences and Peking Union Medical College, Beijing, China

Correspondence
Jianchun Yu, Department of General Surgery, Peking Union Medical College Hospital, No.1 Shuaifuyuan, Dongcheng, Beijing 100730, China.
Email: yu-jch@163.com

Funding information
Beijing Municipal Science and Technology Commission; CAMS Innovation Fund for Medical Sciences

Abstract

Urolithin A (UA) is a microbial metabolite of natural polyphenols ellagitannins and ellagic acid with well-established antitumor properties against various malignancies. However, the exact role of UA in gastric cancer (GC) progression remains largely unclear. In the present study, we investigated the effects and potential mechanisms of UA in GC in vitro and in vivo. Our results revealed that UA could suppress GC cell proliferation, inhibit migration and invasion, promote apoptosis, and induce autophagy via the phosphatidylinositol-3-kinase/protein kinase B/mammalian target of rapamycin pathway in vitro. The autophagy inhibitors 3-methyladenine and chloroquine augmented the inhibitory effect of UA on proliferation and promoted apoptosis, implying that UA mediated the cytoprotective role of autophagy. Meanwhile, the in vivo experiments showed that UA effectively suppressed tumor growth, enhanced the therapeutic effects, and alleviated chemotherapy toxicity in xenograft models. Overall, these findings offer novel insights into the role of UA in tumor therapy and suggest that UA may possess potential therapeutic applications for GC.

KEYWORDS
autophagy, gastric cancer, PI3K/Akt/mTOR pathway, urolithin A

1 | INTRODUCTION

According to the latest global cancer statistics released by the International Agency for Research on Cancer in 2021, gastric cancer (GC) is the fifth most common cancer and the fourth leading cause of cancer-related death globally. GC has a high incidence in China, accounting for 43.9% of new cases worldwide and 48.6% of GC-related deaths (Sung et al., 2021). Notwithstanding that the past decade has witnessed unprecedented progress in diagnosis and treatment approaches for GC, most patients present with advanced-stage disease at initial diagnosis, accounting for the dismal 5-year survival rate (Allemani et al., 2018). D2 gastrectomy combined with perioperative chemotherapy remains the mainstay of treatment for locally advanced GC (Japanese Gastric Cancer Association, 2021; NCCNNetwork, 2020). Accordingly, developing novel drugs for

treating GC is crucial due to tumor resistance and the severe side effects of chemotherapy drugs.

In recent years, research on natural compounds has gained tremendous momentum due to their high bioavailability and limited toxicity. Urolithin A (UA) is one of the major metabolites of natural polyphenols ellagitannins (ETs) and ellagic acid (EA), and is produced by the colon's microbiome-mediated biotransformation (D'Amico et al., 2021). Due to the low absorption within the human gut, the low bioavailability of ETs and EA restricts their efficacy as therapeutic agents. Interestingly, these microbial metabolites are better absorbed than their precursors and are responsible for health activities. There is a growing consensus that UA exerts multiple biological effects such as antiproliferation, proapoptosis, antioxidant, and anti-inflammatory, which play a therapeutic role in numerous diseases, including aging, muscle dysfunctions, cardiovascular or cerebrovascular diseases,

inflammatory diseases, metabolic dysfunctions, and malignancies (Fu et al., 2019; Tang et al., 2017; Totiger et al., 2019; Tuohetaerbaike et al., 2020).

An increasing body of evidence suggests that UA exerts therapeutic effects by regulating the phosphoinositide 3-kinase/protein kinase B (PI3K/Akt) signaling pathway in cancer, osteoarthritis, myocardial ischemia/reperfusion injury, and metabolic diseases (Fu et al., 2019; Tang et al., 2017; Totiger et al., 2019; Tuohetaerbaike et al., 2020). Moreover, UA functions as a potent autophagy activator through diverse pathways in various diseases (Ahsan et al., 2019; Chen et al., 2019; Tuohetaerbaike et al., 2020; Velagapudi et al., 2019; Zhang, Aisker, 2021; Zhang, Zhang, et al., 2021). It has been established that the PI3K/Akt signaling pathway and autophagy participate in multiple cellular functions, which are crucial in tumor genesis and progression. Ample literature suggests that UA exhibits antitumor effects by suppressing the growth of many malignancies, including pancreatic cancer, bladder cancer, colorectal cancer, hepatocellular carcinomas, prostate cancer, lung cancer, and glioblastoma in vitro or vivo (Cheng et al., 2021; Liberal et al., 2017; Liu et al., 2021; Norden & Heiss, 2019; Totiger et al., 2019; Wang et al., 2015; Zhou et al., 2016). However, the mechanism underlying the antitumor effect of UA in GC has hitherto not been reported in the literature.

In the present study, we provided compelling evidence that UA could inhibit proliferation, migration, and invasion, promote apoptosis, and induce cytoprotective autophagy in vitro and in vivo. Moreover, we examined the molecular mechanism underlying the antitumor effects of UA in GC. Our results demonstrated that UA treatment could downregulate the PI3K/Akt/mammalian target of rapamycin (mTOR) pathway in GC cells. Additionally, in a mouse xenograft model, UA effectively suppressed tumor growth, enhanced the therapeutic effects, and alleviated chemotherapy toxicity. Overall, the present study findings provide theoretical and experimental evidence to support the clinical application of UA for human GC treatment, and the combination of UA with autophagy inhibitors may be a more effective therapeutic strategy for GC.

2 | MATERIALS AND METHODS

2.1 | Cell lines and reagents

The human GC cell lines HGC-27 and MKN-45 were obtained from the National Infrastructure of Cell Line Resource, and the human normal gastric epithelium cell line GES-1 was purchased from Procell Life Science & Technology Co., Ltd. Cells were cultured in Roswell Park Memorial Institute (RPMI)-1640 medium supplemented with 10% fetal bovine serum (FBS; Gibco) and 1% penicillin/streptomycin (Gibco) in a humidified atmosphere of 5% CO_2 at 37°C.

UA, 3-methyladenine (3-MA), and chloroquine (CQ) were purchased from Selleck Chemicals. Recombinant human insulin-like growth factor 1 (IGF-1) was purchased from PeproTech.

5-fluorouracil (5-FU) was obtained from Tianjin Jinyao Pharmaceutical Co., Ltd.

2.2 | Cell viability assay

The effect of UA on cell proliferation was detected using Cell Counting Kit-8 (CCK-8; Dojindo) according to the manufacturer's instructions. GC and GES-1 cells were seeded in 96-well plates at a concentration of 3000 cells per well. After incubating overnight, the attached cells were treated with a series of concentrations of UA (0, 5, 10, 20, 50, and 100 μM) for 24 and 48 h. At the indicated time points, the 10 μl CCK-8 solution was added to each well of the plate. After incubation for another 2 h at 37°C, the absorbance was detected at 450 nm using a microplate reader (Bio Tek Epoch). All experiments were repeated five times.

2.3 | Colony formation assay

GC cells were seeded in six-well plates at 1000 cells per well, incubated overnight, and treated with UA (0, 10, and 50 μM) for another 48 h. Then, the culture medium was replaced with a fresh medium every 3 days. After 2 weeks, cells were fixed with 4% paraformaldehyde (Sangon Biotech) for 20 min and stained with 0.1% crystal violet (Sangon Biotech) for 15 min. The number of cell colonies was manually counted after being photographed.

2.4 | 5-Ethynyl-2′-deoxyuridine staining

Cell proliferation was also tested using a 5-ethynyl-2′-deoxyuridine (EdU) Cell Proliferation Kit (Beyotime Biotech). GC cells were seeded in 24-well plates at 3×10^5 cells per well, incubated overnight, and treated with UA (0, 10, and 50 μM) for another 24 h for EdU staining. The cells were then incubated in a culture medium containing 10 μM EdU for 2 h. After fixing with 4% paraformaldehyde (Sangon Biotech) and permeabilizing with 0.3% Triton X-100 (Solaibao), the cells were stained to assess their proliferation following the manufacturer's instructions. Cell nuclei were costained with Hoechst 33342 for 10 min. The cells were imaged using fluorescence microscopy, and the percentage of EdU-positive proliferating cells was determined.

2.5 | Wound healing assay

GC cells were seeded into six-well plates for wound healing assays. After cells grew to 90% confluence, scratches were made across the monolayer of cells by sterile pipette tips. Then, cells were washed three times with phosphate-buffered saline (PBS) to remove exfoliated cells. The remaining cells were incubated in 1% FBS medium with UA (0, 10, and 50 μM) for 24 h at 37°C. The wounds were observed and photographed using a light microscope (Olympus

Corp.), and the area of the wound was measured and analyzed using Image J software (NIH).

2.6 | Transwell migration and invasion assays

Cell migration and invasion assays were conducted using the 24-well Transwell chambers (8 μM pore size; Corning Costar). For the invasion assay, the upper chambers were precoated with Matrigel (1:8, diluted with serum-free RPMI-1640 medium; BD Biosciences). Following treatment with UA (0, 20 μM) for 24 h, HGC-27 and MKN-45 cells (8×10^4 for migration or 1×10^5 for invasion) in 200 μl suspension containing 1% FBS were seeded to the upper chambers, while 500 μl medium containing 20% FBS was added in the lower chambers. After 24 h of incubation at 37°C, cells remaining on the upper surface of the chamber were removed with cotton swabs. Then, cells that passed through the membrane and attached to the lower surface were fixed in 4% paraformaldehyde (Sangon Biotech) for 20 min, and stained with 0.1% crystal violet (Sangon Biotech) for 15 min. The stained migrated or invaded cells were photographed and counted using a light microscope in five random fields (Olympus Corp.).

2.7 | Cell apoptosis assay

Cell apoptosis detection was conducted using the Annexin V, 633 Apoptosis Detection Kit (Dojindo). For apoptosis assay, GC cells were seeded at 1×10^6 cells in six-well plates, incubated overnight, and treated with UA (0, 20, and 50 μM) for another 24 h. Then, The cells were harvested by trypsinization gently, washed twice with cold PBS, and resuspended in the binding buffer. Furthermore, cells were stained with 5 μl Annexin V and 5 μl propidium iodide (PI) for 15 min in the dark. Each sample was detected by flow cytometry with at least 20,000 cells (BD Accuri C6 Plus; BD Biosciences) within 1 h. The percentage of live, early apoptotic, late apoptotic, and necrotic cells were calculated and analyzed using Flowjo software.

2.8 | Western blot and antibodies

Cells were lysed to extract total protein using radioimmunoprecipitation assay lysis and extraction buffer (Thermo Fisher Scientific) with protease and phosphatase inhibitor cocktail (Thermo Fisher Scientific) for 15 min on ice. Protein lysates were centrifuged at 14,000g for 15 min at 4°C to collect the supernatant. The protein concentration was measured by Enhanced BCA Protein Assay Kit (Beyotime) following the manufacturer's protocol. Protein lysates were denatured and subjected to 10% sodium dodecyl sulfate-polyacrylamide gel electrophoresis. Loading controls were analyzed on each separate gel. Thereafter, proteins were transferred onto polyvinylidene fluoride membranes (Millipore). After blocking with 5% nonfat milk for 2 h at room temperature, the membranes were incubated with primary antibodies at 4°C overnight. Membranes were subsequently rinsed and incubated with corresponding horseradish peroxidas-conjugated secondary antibodies (1:10,000; Cell Signaling Technology) at room temperature for 1 h. The protein bands were detected and visualized using SuperSignal West Pico PLUS Chemiluminescent Substrate (Thermo Fisher Scientific). The following primary antibodies were used in this study: anti-phospho-AKT (S473) (1:1000; Cell Signaling Technology), anti-AKT (1:1000; Cell Signaling Technology), anti-phospho-mTOR (S2448) (1:1000; Cell Signaling Technology), anti-mTOR (1:1000; Cell Signaling Technology), anti-phospho-p70S6K (T421/S424) (1:1000; ABclonal), anti-p70S6K (1:1000; ABclonal), anti-phospho-S6 (S235/236) (1:1000; ABclonal), anti-S6 (1:1000; ABclonal), anti-LC3 (1:1000; Cell Signaling Technology), anti-p62 (1:1000; ABclonal), anti-Bax (1:1000; ABclonal), anti-Bcl-2 (1:1000; ABclonal), and anti-β-actin (1:1000; Cell Signaling Technology).

2.9 | Transmission electron microscopy

HGC-27 and MKN-45 cells were seeded in 10 cm culture dishes and treated with UA (0 and 50 μM) for 6 h. The cells were fixed with 2.5% glutaraldehyde, scraped off the culture plates, and centrifuged at 1500 rpm for 2 min. After fixation, specimens were kept at 4°C before agarose pre-embedding. Then, the samples were postfixed with 1% OsO4 in 0.1 M phosphate buffer (pH 7.4) for 2 h at room temperature. After dehydration with graded alcohol and acetone, the samples were infiltrated, embedded, and polymerized in ethoxyline resin. The ultrathin sections (60–80 nm) were obtained with an ultramicrotome (Leica UC7; Leica) and stained with 2% uranium acetate and lead citrate. The autophagic microstructures were observed and photographed using a transmission electron microscope (TEM; HT7800; Hitachi Scientific Instruments).

2.10 | Immunofluorescence staining

Cells were cultivated on climbing slices, and incubated with UA (0 and 50 μM) for 24 h. For immunostaining, cells were fixed with 4% paraformaldehyde (Sangon Biotech) for 30 min, then blocked with 3% bovine serum albumin (BSA; Servicebio) for 30 min. Next, the cells were incubated with an anti-LC3 antibody at 4°C overnight. Following this, cells were incubated with secondary antibodies for 1 h, and the nuclei of cells were counterstained with 4′,6-diamidino-2-phenylindole (Servicebio) for 10 min. After the anti-fluorescence quenching seal, images were captured using a fluorescence microscope (NIKON ECLIPSE C1 and NIKON DS-U3).

2.11 | RNA-sequencing analysis

After treatment with UA (0 and 50 μM) for 24 h, the total RNA was extracted using TRIzol reagent (Invitrogen) according to the

manufacturer's instructions, and genomic DNA contamination was removed with RNase-free DNase I. RNA integrity, quality, and quantity were detected sequentially. The high RNA samples were submitted for library preparation and sequencing (Sangon Biotech). RNA-sequencing analysis was performed using MGISEQ-2000 (MGI). Functional enrichment analyses were carried out, including Gene Ontology (GO) and the Kyoto Encyclopedia of Genes and Genomes (KEGG). Differentially expressed genes (DEGs) underwent GO annotation in terms of biological process, cellular component, and molecular function. The KEGG pathway enrichment analysis identified significantly enriched metabolic pathways or signal transduction pathways associated with DEGs. GO terms and KEGG pathways with $p < .05$ were considered significantly enriched.

2.12 | Mouse xenograft model

Male BALB/C nude mice (5-week-old) were purchased from Charles River. The mice were randomly divided into four groups ($n = 5$ per group), control, UA, 5-FU, and UA + 5-FU. 5×10^6 MKN-45 cells were resuspended in 100 µl precooled PBS and subcutaneously injected into the right flank of nude mice. When the tumor volume reached 100 mm^3, the mice received UA (20 mg/kg/day, 6 days/week, oral gavage) or 5-FU (30 mg/kg, twice a week, intraperitoneal injection) according to indicated assay. Tumor volumes and body weight of mice were measured using a digital caliper and electronic scale every 3 days, respectively. The tumor volume was calculated according to the following formula: volume = length × width^2/2. After 3 weeks, the mice were killed, and tumors were removed, weighed, and fixed with paraformaldehyde (Servicebio) for immunohistochemistry (IHC). All animal experiments followed the protocols approved by the Ethics Committee of Animal Experiments of Peking Union Medical College Hospital.

2.13 | Immunohistochemistry

Tissue samples fixed with paraformaldehyde were embedded in paraffin and sectioned. Routine histological examination and morphological analyses were performed with hematoxylin and eosin staining. For IHC staining, the sections were dewaxed, hydrated, and underwent antigen repair. After blocking with 3% BSA (Servicebio), sections were incubated with primary antibodies against human Ki67, cleaved caspase-3, LC3, and phospho-AKT (S473) overnight at 4°C. After washing with PBS, a secondary antibody was added and incubated for 1 h at room temperature. The sections were stained with diaminobenzidine (Servicebio), and nuclei counterstained with hematoxylin (Servicebio).

2.14 | Statistical analysis

All experiments were repeated at least three times independently. Data were presented as the mean ± standard deviation (SD). The statistical analyses were conducted using GraphPad Prism 8 (GraphPad Prism Software Inc.). Different groups were analyzed using Student's t-test. p values less than .05 were considered statistically significant.

3 | RESULTS

3.1 | UA suppresses the proliferation of GC cells

To investigate whether UA could suppress cell growth, HGC-27 and MKN-45 cells were treated with a series of concentrations of UA (0, 5, 10, 20, 50, and 100 µM) for 24 and 48 h, and cell viability was detected using the CCK-8 assay. These results revealed that UA could significantly inhibit the proliferation of HGC-27 and MKN-45 cells in a dose- and time-dependent manner (Figure 1a). However, the viability of GES-1 cells was minimally affected after UA treatment at the same concentrations, highlighting the specificity of UA for GC cells (Figure 1b). The colony formation and EdU staining assays consistently showed that UA could inhibit cell proliferation. As expected, a decreased proportion of EdU-positive cells was observed after UA treatment (Figure 1c). Colony formation assays also showed a dramatic reduction in the number of colonies after UA treatment in a dose-dependent manner (Figure 1d). Taken together, these data suggested that UA could suppress cell growth and proliferation in GC cells.

3.2 | UA inhibits the migration and invasion of GC cells

To examine the effects of UA on the migratory and invasive capacities of GC cells, wound healing and Transwell experiments were performed. The wound healing assay indicated that the migration of GC cells was significantly reduced under UA treatment in a concentration-dependent manner (Figure 1e). Moreover, in the Transwell assays, the number of migrated and invaded cells was significantly decreased in the HGC-27 and MKN-45 groups exposed to UA (Figure 1f,g). These data suggested that UA could inhibit the migration and invasion of GC cells.

3.3 | UA promotes apoptosis in GC cells

To explore whether the inhibitory effect of UA on GC cell proliferation was related to apoptosis, apoptotic cell death was evaluated by Apoptosis Detection Kit. HGC-27 and MKN-45 cells were treated with different concentrations of UA, stained with Annexin V/633 and PI, and detected apoptosis by flow cytometry. Following 24 h of treatment, both early and late apoptotic cells were significantly increased with the increasing UA dose (Figure 1h). Furthermore, UA-induced apoptosis was confirmed by upregulated proapoptotic protein Bax expression and downregulated antiapoptotic protein Bcl-2 expression in a dose-dependent manner in HGC-27
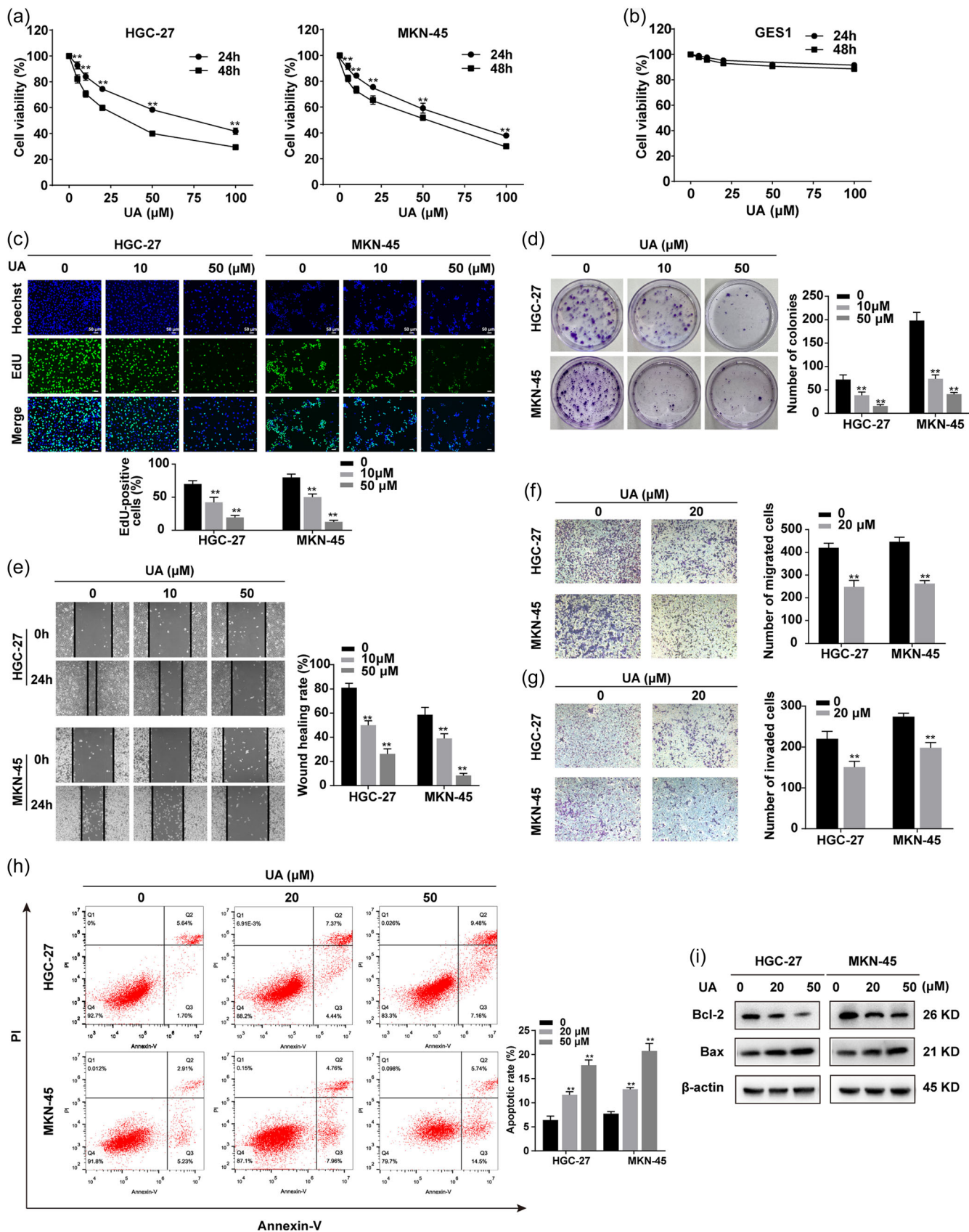
FIGURE 1 (See caption on next page)

and MKN-45 cells (Figure 1i). These results demonstrated that UA could induce cell apoptosis in human GC cells in a dose-dependent manner.

3.4 | UA induces autophagy in GC cells

To explore whether UA regulates autophagy in GC cells, TEM analysis was performed to observe the autophagic microstructures. The results showed that the formation of autophagic vacuoles in UA-treated cells was dramatically increased (Figure 2a). Immuno-fluorescent staining revealed that the quantity of LC3 fluorescent puncta was increased after UA treatment (Figure 2b). Western blot assays confirmed an increased level of LC3 II/LC3 I (a marker of autophagic activity and autophagosome formation) in a dose-dependent manner (Figure 2c). Additionally, compared with the control, a decrease in p62 expression was observed following UA treatment. As a ubiquitin-binding protein, p62 can reportedly interact with LC3-II and be degraded during autophagy (Figure 2c). To further confirm UA-induced autophagy, 3-MA (an autophagosome formation inhibitor) and CQ (an inhibitor of lysosome-autophagosome fusion) were used to block the early and late phases of autophagy, respectively. The results showed that the stimulatory effect of UA on LC3-II accumulation was suppressed in the presence of 3-MA (Figure 2d). Furthermore, cotreatment with CQ significantly increased UA-induced LC3-II accumulation (Figure 2e), substantiating that autophagy occurred in UA-treated GC cells.

Growing evidence suggests that autophagy yields cytoprotective or cytotoxic effects depending on the cellular stress level and treatment response, indicating that autophagy can be either tumor-suppressive or stimulatory (Gewirtz, 2014). In the present study, two autophagy inhibitors, 3-MA and CQ, were used to block the autophagy process and explore the role of UA-induced autophagy in cell viability and apoptosis. CCK-8 assays revealed that the combination of UA with 3-MA or CQ could augment the inhibitory effect of UA on cell viability compared with UA treatment alone (Figure 3a,b). Moreover, apoptosis assays showed that the combination of UA with 3-MA or CQ significantly increased the proportion of apoptotic cells (Figure 3c,d). Western blot further demonstrated that autophagy inhibitors increased the expression of proapoptotic protein Bax and reduced the expression of antiapoptotic protein Bcl-2 compared to those treated only with UA (Figure 3e,f). Taken together, these results suggested that UA treatment induces cytoprotective autophagy in GC cells.

3.5 | UA inhibits the PI3K/Akt/mTOR pathway in GC cells

An increasing body of evidence suggests that inhibition of PI3K/AKT/mTOR activation suppresses GC growth and negatively regulates autophagy (He & Klionsky, 2009; Russell et al., 2014). RNA sequencing analysis also revealed that the PI3K–Akt signaling pathway mediated the antitumor effects of UA on GC cells (Supporting Information: Figure S1). On the basis of the above results, we examined the influence of UA on the PI3K/Akt/mTOR pathway in GC cells. Western blot assays revealed that GC cells treated with UA reduced the phosphorylation level of Akt, mTOR, p70S6K, and S6 in a dose-dependent manner, while no significant alternations were detected in the levels of total Akt, mTOR, p70S6K, and S6 (Figure 4a). To further confirm whether the PI3K/Akt/mTOR pathway is involved in UA-mediated antitumor effects in GC cells, cells were treated with UA and IGF-1 (PI3K activator). Compared with UA treatment alone, phosphorylation of Akt, mTOR, p70S6K, and S6 inhibited by UA was reversed by pretreatment with IGF-1 (Figure 4b). In addition, IGF-1 treatment attenuated the UA-induced LC3-II accumulation (Figure 4b). Overall, these findings suggested that UA suppresses GC growth and induces autophagy by inhibiting the PI3K/Akt/mTOR pathway.

3.6 | UA suppresses tumor growth in vivo

To further investigate the effects of UA on tumor growth in vivo, we used MKN-45 cells to establish xenograft models in nude mice. Given that 5-FU is the first-line chemotherapy drug for GC, it was selected as a positive control to validate the antitumor activity of UA in vivo. We found that tumor volume and weight were significantly decreased in the UA and 5-FU groups compared with the controls. Interestingly, compared with 5-FU treatment alone, UA combined with 5-FU led to a more significant reduction in tumor volume and weight (Figure 5a–c). Furthermore, the combination of UA and 5-FU could reduce chemotherapy toxicity, evidenced by less weight loss during therapy (Figure 5d). IHC staining of tumor tissue revealed that the expression

FIGURE 1 UA suppresses proliferation, inhibits migration and invasion, and promotes apoptosis of GC cells. (a, b) GC cells and normal gastric mucosal cells GES-1 were treated with a series of concentrations (0, 5, 10, 20, 50, and 100 μM) of UA for 24 and 48 h. Cell viability was detected by the CCK-8 assay. (c) EdU staining was performed to test cell proliferation rates of GC cells treated with UA (0, 10, and 50 μM) for 24 h. Blue, Hoechst; green, EdU. Scale bar = 50 μm. (d) The abilities of GC cells to form colonies were detected after treatment with the indicated concentrations (0, 10, and 50 μM) of UA. (e) A wound healing assay was conducted to assess the effect of UA (0, 10, and 50 μM) on the migration of GC cells 24 h after treatment. (f, g) Migration and invasion capacity of GC cells treated with UA (0 and 20 μM) were assessed by Transwell assays. (h) GC cells were treated with UA (0, 20, and 50 μM) for 24 h, stained with Annexin V-633/PI, and analyzed for apoptosis using flow cytometry. (i) Cells were treated with the UA (0, 20, and 50 μM) for 24 h, and the Bcl-2 and Bax protein expression were analyzed by Western blot. Data were presented as mean ± SD. $*p < .05$; $**p < .01$ versus the control. CCK-8, Cell Counting Kit-8; EdU, 5-ethynyl-2′-deoxyuridine; GC, gastric cancer; PI, propidium iodide; UA, urolithin A.
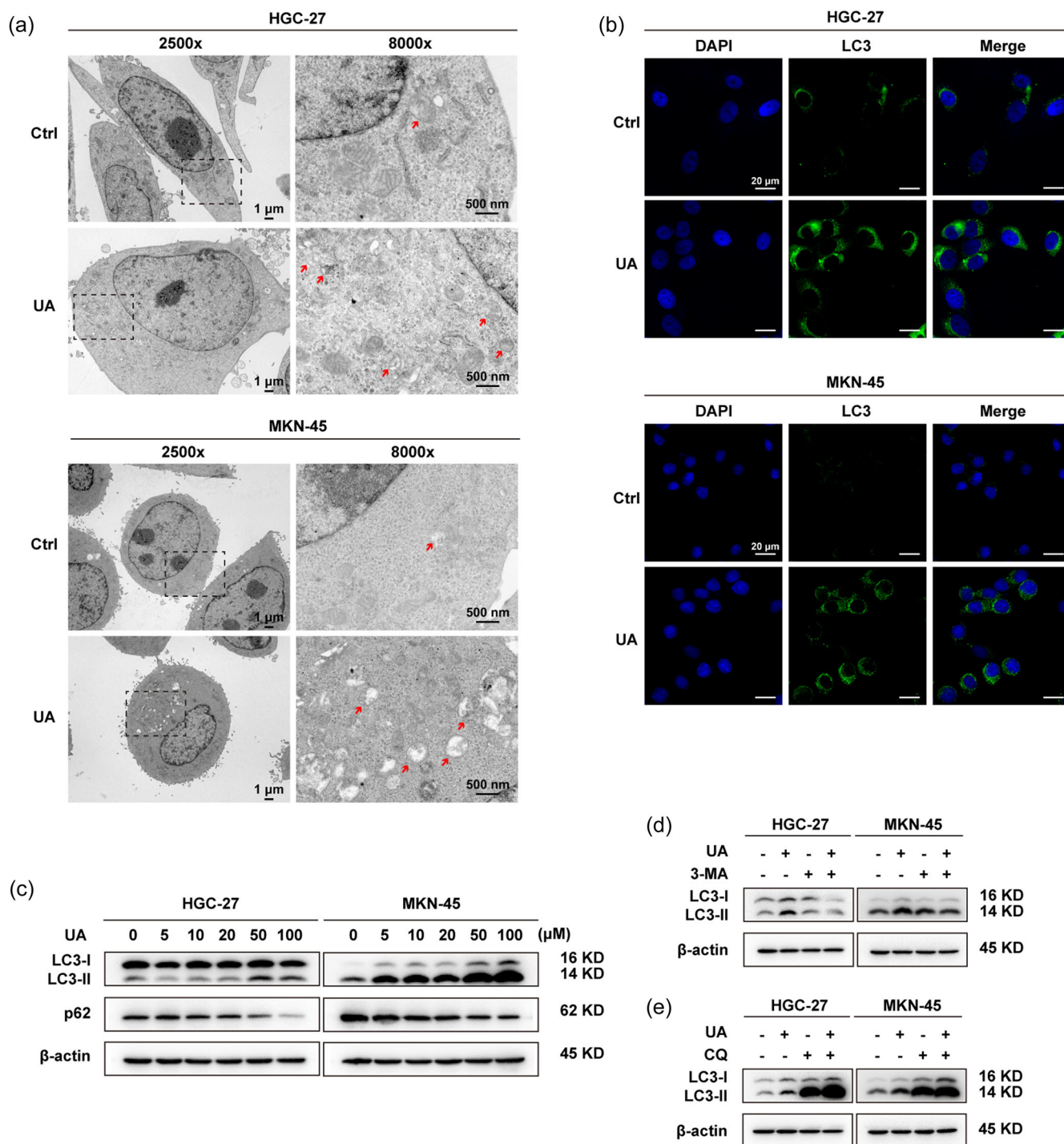
FIGURE 2 UA induces autophagy in GC cells. (a) Transmission electron microscopy analysis revealed the autophagic microstructures of HGC-27 and MKN-45 cells after treatment with UA (0 and 50 μM) for 6 h. Representative autophagic vacuoles (red arrows) in HGC-27 and MKN-45 cells are highlighted in the enlarged images. Magnification, ×2500, scale bar = 1 μm; magnification, ×8000, scale bar = 500 nm. (b) After treatment with UA (0, 50 μM), HGC-27 and MKN-45 cells were stained with anti-LC3 antibodies for observation of LC3 puncta formation by immunofluorescence. Blue, DAPI; Green, LC3. Scale bar = 20 μm. (c) HGC-27 and MKN-45 cells were stimulated with the indicated concentration (0, 5, 10, 20, 50, and 100 μM) of UA for 24 h. Autophagy-related proteins LC3 and p62 were detected by Western blot. (d, e) HGC-27 and MKN-45 cells were preincubated with 3-MA (5 mM) or CQ (50 μM) for 2 h and then treated with UA (50 μM) for 24 h. Detection of LC3 protein levels by Western blot. 3-MA, 3-methyladenine; CQ, chloroquine; Ctrl, control; DAPI, 4′,6-diamidino-2-phenylindole; GC, gastric cancer; UA, urolithin A.
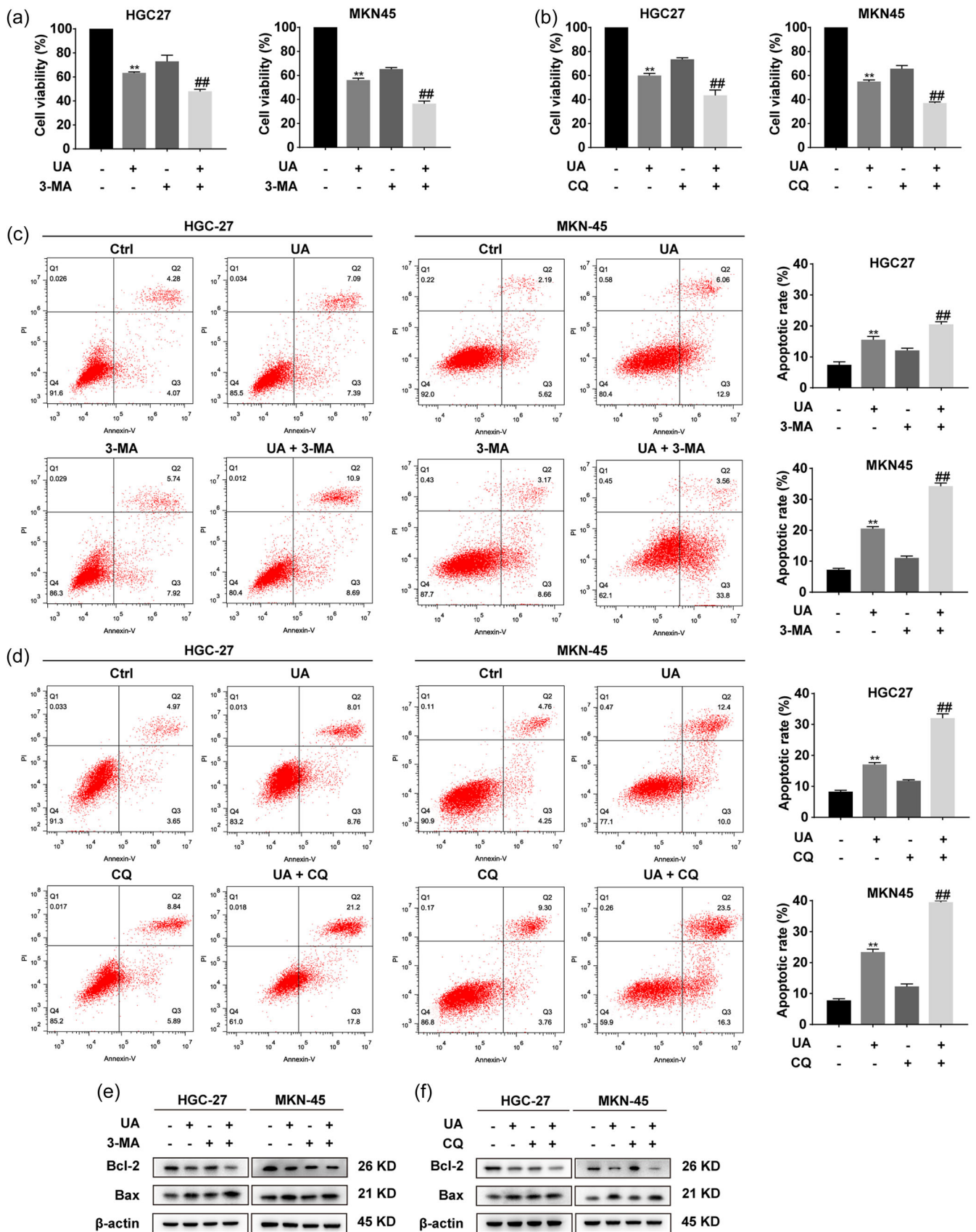
WILEY

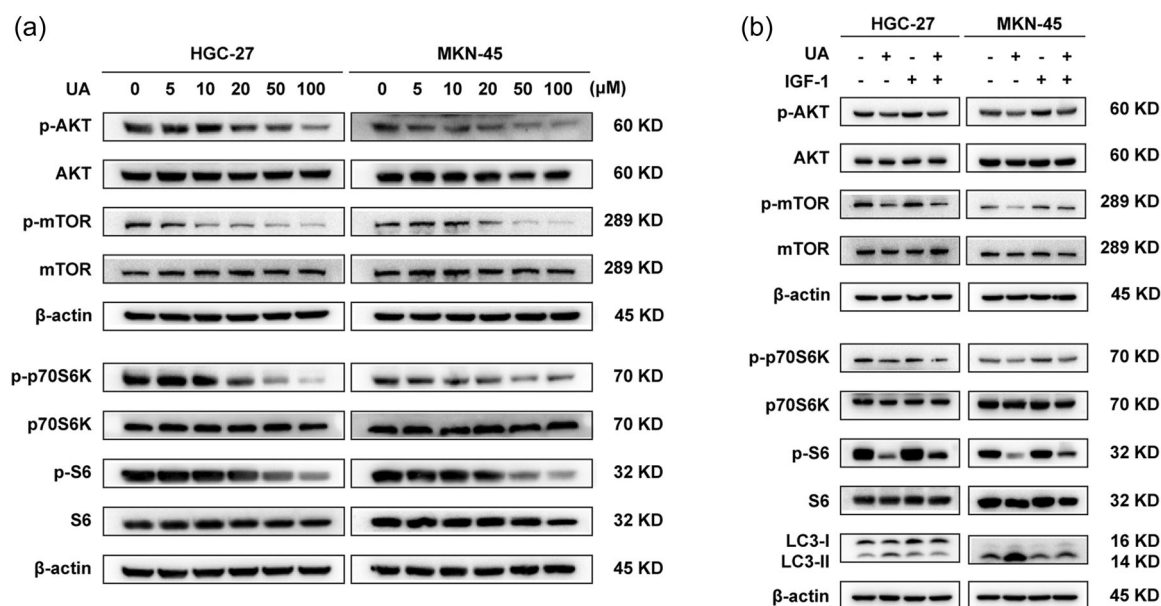**FIGURE 3** (See caption on next page)

FIGURE 4 UA treatment downregulates the PI3K/Akt/mTOR pathway in GC cells. (a) HGC-27 and MKN-45 cells were treated with the indicated concentration (0, 5, 10, 20, 50, and 100 μM) of UA, and then the expression levels of p-AKT, AKT, p-mTOR, mTOR, p-p70S6K, p70S6K, p-S6, and S6 were detected by Western blot. (b) GC cells were treated with UA (50 μM) in the absence or presence of IGF-1 (100 ng/ml). The expression of proteins associated with the PI3K/Akt/mTOR pathway and autophagy were detected by Western blot. AKT, protein kinase B; GC, gastric cancer; IGF-1, insulin-like growth factor 1;mTOR, mammalian target of rapamycin pathway; PI3K, phosphatidylinositol-3-kinase; p-AKT, phospho-AKT; p-mTOR, phospho-mTOR; UA, urolithin A.

of Ki67 and p-AKT were decreased, while the expression of Cleaved Caspase-3 and LC3 was increased in UA-treated and UA + 5-FU-treated groups (Figure 5e). Taken together, these results demonstrated that UA could suppress tumor growth, enhance the therapeutic effects, and alleviate the toxicity of 5-FU in vivo.

4 | DISCUSSION

GC is a major life-threatening malignancy with high morbidity and mortality rates. Surgery resection plays a vital role in treating GC, while neoadjuvant/adjuvant chemotherapy is generally recommended for locally advanced GC (X. Zhang et al., 2021). These findings highlight the importance of the quest to discover and develop novel anticancer agents with high efficacy, low toxicity, and minimal side effects. The present study showed that the antitumor effects of UA were mediated by inhibiting cell proliferation, migration, and invasion, and promoting apoptosis via the PI3K/Akt/mTOR pathway. Moreover, UA-induced autophagy played a

cytoprotective role against UA-induced proliferation inhibition and apoptosis promotion in GC cells. To our knowledge, this is the first study to investigate the effects of UA in GC in vitro and in vivo.

UA is a microbial metabolite of the natural compounds (ETs and EA) found in pomegranates, berries, and nuts (D'Amico et al., 2021). There is a rich literature available substantiating that UA yields therapeutic effects against multiple types of malignancies, which provides a potential and promising strategy for tumor treatment. UA is known to mediate antitumor activity by targeting multiple signaling pathways, including p-53 pathways, PI3K/Akt signaling, Wnt signaling, mitogen-activated protein kinases signaling, extracellular signal-regulated kinase pathways, and autophagy (El-Wetidy et al., 2021; Liu et al., 2021; Norden & Heiss, 2019; Sharma et al., 2010; Totiger et al., 2019). Of note, Totiger et al. (2019) documented that UA treatment on pancreatic ductal adenocarcinoma suppressed tumor cell proliferation and immunosuppressive cell recruitment. In addition, UA has been reported to potentiate the anticancer effect of 5-FU in colon cancer cells by inducing cell cycle arrest and apoptosis (González-Sarrías et al., 2015). Based on these findings, we designed

FIGURE 3 Blocking autophagy induced by UA augmented the effect of UA on suppressing proliferation and promoting apoptosis on GC cells. HGC-27 and MKN-45 cells were preincubated with 3-MA (5 mM) or CQ (50 μM) for 2 h and then treated with UA (50 μM) for 24 h. (a, b) Cell viability was determined by CCK-8 assays. (c, d) Proportions of apoptotic cells were determined by Annexin V-PI staining. (e, f) Detection of Bcl-2 and Bax protein levels by Western blot. Data were presented as mean ± SD. **$p < .01$ versus the control; ##$p < .01$ versus the cells treated only with UA. 3-MA, 3-methyladenine; CCK-8, Cell Counting Kit-8; CQ, chloroquine; Ctrl, control; GC, gastric cancer; PI, propidium iodide; UA, urolithin A.
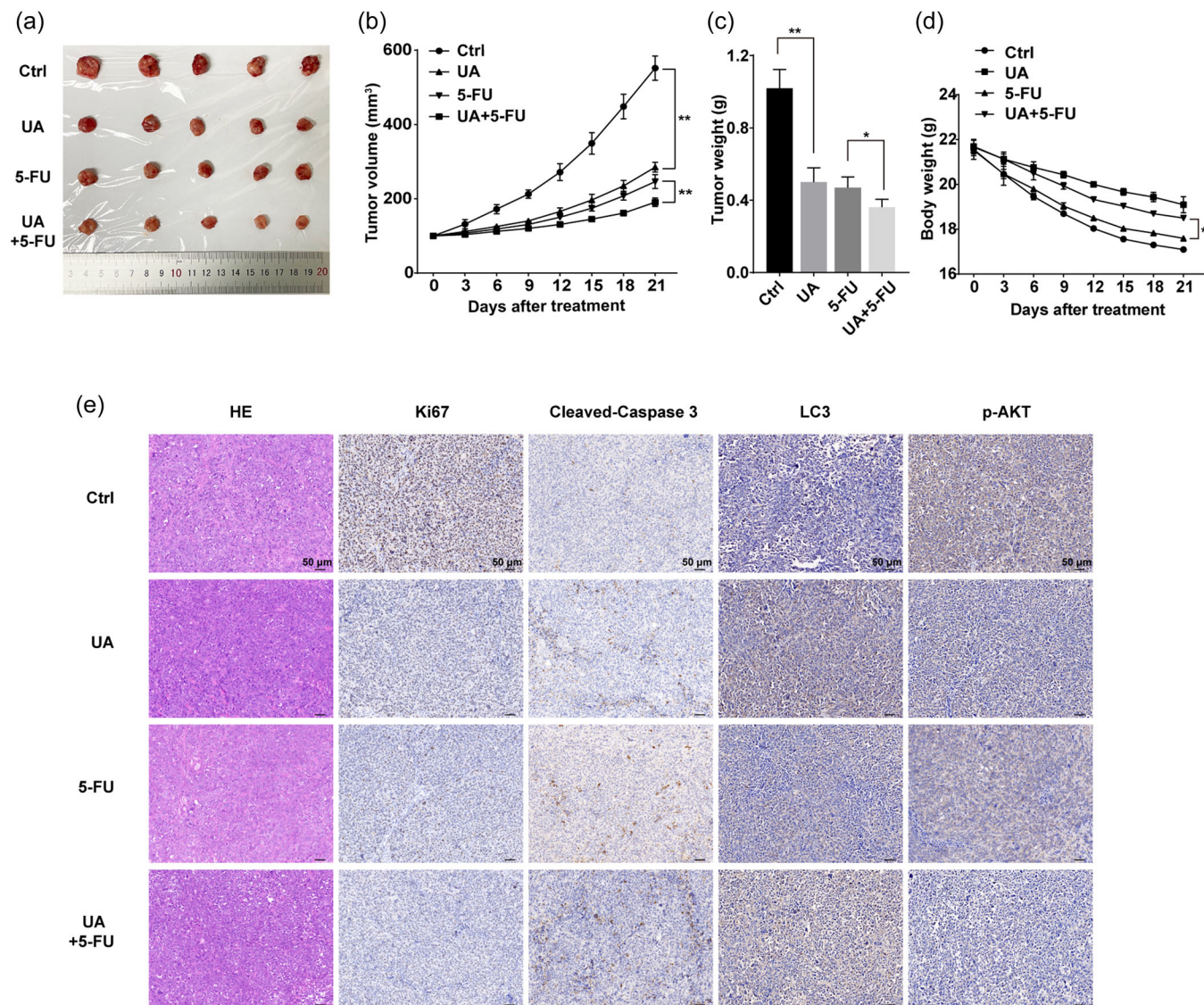
FIGURE 5 UA suppresses tumor growth in vivo. (a) After 21 days of treatment, the mice were killed, and tumors were removed and photographed. (b) Tumor volumes were measured every 3 days. (c) Tumor weights were calculated. (d) Mice's body weights were monitored. (e) Representative IHC staining images of HE, Ki67, cleaved-caspase 3, LC3, and p-AKT were shown for every group. Scale bar = 50 μm. Data were presented as mean ± SD. *$p < .05$; **$p < .01$ versus the control or 5-FU group. 5-FU, 5-fluorouracil; Ctrl, control; HE, hematoxylin and eosin; IHC, immunohistochemistry; p-AKT, phospho-protein kinase B; UA, urolithin A.

a series of experiments to explore the role of UA and its potential clinical application in GC. Our results indicated that UA exerts antitumor activities by inhibiting proliferation, migration, and invasion, promoting apoptosis, and enhancing the chemotherapy effects in GC in vitro and in vivo. Furthermore, UA-induced cytoprotective autophagy in GC cells. According to the sequencing results, UA suppresses tumor progression and induces autophagy in GC via the PI3K/Akt/mTOR pathway. Overall, the above findings validate that UA might be a promising therapeutic agent in GC, and the combination of UA with autophagy inhibitors may be a more effective therapeutic strategy for GC.

Growing evidence suggests that many anticancer agents can induce autophagy in multiple types of malignancies, indicating that

targeting autophagy has huge prospects as a therapeutic strategy for cancer. The process of autophagy involves lysosomal degradation, which is vital for survival, differentiation, development, and homeostasis (Levine & Kroemer, 2008). Autophagy reportedly plays a dual role in tumorigenesis and tumor progression. On one hand, as a tumor suppressor, autophagy prevents the accumulation of damaged proteins/organelles and limits cellular growth and genomic instability. On the other hand, autophagy-related stress tolerance can help tumor cells adapt to increased metabolic demands, hypoxic microenvironment, or tumor therapy (Yang et al., 2011). Interestingly, the cytoprotective role of autophagy has been reported to contribute to chemoresistance or targeted drug resistance during progressive disease (Gewirtz, 2014). Hence, interfering with cytoprotective
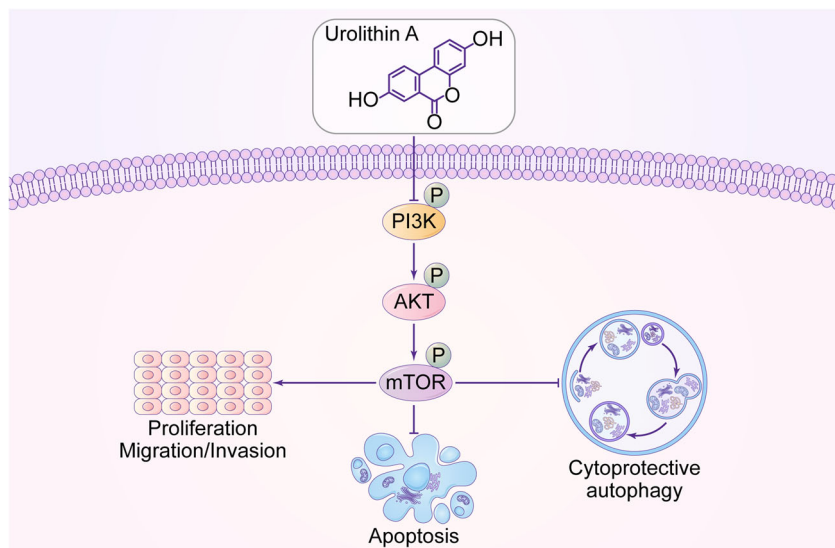
FIGURE 6 Schematic diagram of the molecular mechanism by which urolithin A exerts antitumor effects in gastric cancer. AKT, protein kinase B; mTOR, mammalian target of rapamycin pathway; PI3K, phosphatidylinositol-3-kinase.

autophagy helps us to enhance drug sensitivity. It is of great importance to rationally control autophagy for tumor therapy. An overwhelming body of literature substantiates that UA has protective effects on the pancreas, kidney, and nervous system through autophagy activation (Ahsan et al., 2019; Chen et al., 2019; Tuohetaerbaike et al., 2020; Velagapudi et al., 2019; Zhang, Aisker, et al., 2021; Zhang, Zhang, et al., 2021). As far as we know, this is the first study indicating that UA could induce autophagy in GC cells. UA treatment promotes LC3-II accumulation, reduces the expression of p62, and triggers autophagosome formation in GC cells. Moreover, a disruption in UA-induced autophagy by 3-MA and CQ caused significant synergistic antitumor effects in GC cells, as evidenced by the significantly decreased cell viability and increased apoptosis rate. These data substantiate that UA-induced autophagy might play a cytoprotective role in GC cells, and the combination treatment of UA and autophagy inhibitors might be more effective for GC therapy if UA is used clinically in the future.

The PI3K/Akt/mTOR pathway is a key signaling cascade for cell survival, proliferation, differentiation, apoptosis, and metabolism and is reportedly activated in tumor initiation, progression, metastasis, and drug resistance (Engelman, 2009; Fruman & Rommel, 2014). This signaling pathway has been reported to be aberrantly activated in various malignancies, including GC (Huang et al., 2019). PI3K is activated through ligand binding and subsequently phosphorylates Akt and activates downstream pathways, including mTOR, which promotes cellular proliferation, inhibits apoptosis and autophagy, and reduces sensitivity to chemotherapeutic agents (Engelman, 2009; Fruman & Rommel, 2014). In addition, the mTOR complex plays a negative role in autophagy and inhibits the formation of autophagosomes by activating p70S6K (He & Klionsky, 2009). Thus, this signaling pathway has become a vital therapeutic target for GC treatment. Indeed, the relationship between UA and the PI3K/Akt pathway has been documented in pancreatic and bladder cancers (Liberal et al., 2017; Totiger et al., 2019). In this study, tumor suppression and autophagy induced by UA were mediated by the PI3K/Akt/mTOR pathway, as

evidenced by the downregulated expression of the phosphorylated Akt, mTOR, and p70S6K. Furthermore, activation of the PI3K/Akt/mTOR pathway by IGF-1 attenuated UA-induced autophagy in GC cells. These results revealed that downregulation of the PI3K/Akt/mTOR pathway represented a vital molecular mechanism by which UA suppresses tumor progression in GC (Figure 6).

5 | CONCLUSION

In conclusion, our study demonstrates that UA could suppress proliferation, inhibit migration and invasion, promote GC cell apoptosis in vitro, and inhibit tumor growth in vivo. Furthermore, UA could trigger protective autophagy by blocking PI3K/Akt/mTOR pathway in GC. Importantly, the present study provides the theoretical and experimental basis for the clinical application of UA in GC. Additionally, our findings improve our current understanding of the antitumor properties of UA and substantiate that UA has huge prospects for clinical application in GC patients.

CONFLICT OF INTEREST

The authors declare no conflict of interest.

DATA AVAILABILITY STATEMENT

The data that support the findings of this study are available from the corresponding author upon reasonable request.

ORCID

Jianchun Yu 🆔 http://orcid.org/0000-0002-8250-7475

REFERENCES

Ahsan, A., Zheng, Y. R., Wu, X. L., Tang, W. D., Liu, M. R., Ma, S. J., Jiang, L., Hu, W. W., Zhang, X. N., & Chen, Z. (2019). Urolithin A-activated autophagy but not mitophagy protects against ischemic neuronal injury by inhibiting ER stress in vitro and in vivo. CNS Neuroscience & Therapeutics, 25(9), 976–986. https://doi.org/10.1111/cns.13136

Allemani, C., Matsuda, T., Di Carlo, V., Harewood, R., Matz, M., Nikšić, M., Bonaventure, A., Valkov, M., Johnson, C. J., Estève, J., Ogunbiyi, O. J., Azevedo e Silva, G., Chen, W. Q., Eser, S., Engholm, G., Stiller, C. A., Monnereau, A., Woods, R. R., Visser, O., ... Hood, M. (2018). Global surveillance of trends in cancer survival 2000–14 (CONCORD-3): Analysis of individual records for 37 513 025 patients diagnosed with one of 18 cancers from 322 population-based registries in 71 countries. The Lancet, 391(10125), 1023–1075. https://doi.org/10.1016/s0140-6736(17)33326-3

Chen, P., Chen, F., Lei, J., Li, Q., & Zhou, B. (2019). Activation of the miR-34a-Mediated SIRT1/mTOR signaling pathway by urolithin A attenuates D-galactose-induced brain aging in mice. Neurotherapeutics, 16(4), 1269–1282. https://doi.org/10.1007/s13311-019-00753-0

Cheng, F., Dou, J., Zhang, Y., Wang, X., Wei, H., Zhang, Z., Cao, Y., & Wu, Z. (2021). Urolithin A inhibits epithelial-mesenchymal transition in lung cancer cells via P53-Mdm2-Snail pathway. OncoTargets and Therapy, 14, 3199–3208. https://doi.org/10.2147/ott.S305595

D'Amico, D., Andreux, P. A., Valdés, P., Singh, A., Rinsch, C., & Auwerx, J. (2021). Impact of the natural compound urolithin A on health, disease, and aging. Trends in Molecular Medicine, 27, 687–699. https://doi.org/10.1016/j.molmed.2021.04.009

El-Wetidy, M. S., Ahmad, R., Rady, I., Helal, H., Rady, M. I., Vaali-Mohammed, M. A., Al-Khayal, K., Traiki, T. B., & Abdulla, M. H. (2021). Urolithin A induces cell cycle arrest and apoptosis by inhibiting Bcl-2, increasing p53-p21 proteins and reactive oxygen species production in colorectal cancer cells. Cell Stress and Chaperones, 26(3), 473–493. https://doi.org/10.1007/s12192-020-01189-8

Engelman, J. A. (2009). Targeting PI3K signalling in cancer: Opportunities, challenges and limitations. Nature Reviews Cancer, 9(8), 550–562. https://doi.org/10.1038/nrc2664

Fruman, D. A., & Rommel, C. (2014). PI3K and cancer: Lessons, challenges and opportunities. Nature Reviews Drug Discovery, 13(2), 140–156. https://doi.org/10.1038/nrd4204

Fu, X., Gong, L. F., Wu, Y. F., Lin, Z., Jiang, B. J., Wu, L., & Yu, K. H. (2019). Urolithin A targets the PI3K/Akt/NF-κB pathways and prevents IL-1β-induced inflammatory response in human osteoarthritis: In vitro and in vivo studies. Food & Function, 10(9), 6135–6146. https://doi.org/10.1039/c9fo01332f

Gewirtz, D. A. (2014). The four faces of autophagy: Implications for cancer therapy. Cancer Research, 74(3), 647–651. https://doi.org/10.1158/0008-5472.Can-13-2966

González-Sarrías, A., Tomé-Carneiro, J., Bellesia, A., Tomás-Barberán, F. A., & Espín, J. C. (2015). The ellagic acid-derived gut microbiota metabolite, urolithin A, potentiates the anticancer effects of

5-fluorouracil chemotherapy on human colon cancer cells. Food & Function, 6(5), 1460–1469. https://doi.org/10.1039/c5fo00120j

He, C., & Klionsky, D. J. (2009). Regulation mechanisms and signaling pathways of autophagy. Annual Review of Genetics, 43, 67–93. https://doi.org/10.1146/annurev-genet-102808-114910

Huang, Y., Kang, W., Ma, Z., Liu, Y., Zhou, L., & Yu, J. (2019). NUCKS1 promotes gastric cancer cell aggressiveness by upregulating IGF-1R and subsequently activating the PI3K/Akt/mTOR signaling pathway. Carcinogenesis, 40(2), 370–379. https://doi.org/10.1093/carcin/bgy142

Japanese Gastric Cancer Association. (2021). Japanese gastric cancer treatment guidelines 2018 (Vol. 24, 5th ed.).

Levine, B., & Kroemer, G. (2008). Autophagy in the pathogenesis of disease. Cell, 132(1), 27–42. https://doi.org/10.1016/j.cell.2007.12.018

Liberal, J., Carmo, A., Gomes, C., Cruz, M. T., & Batista, M. T. (2017). Urolithins impair cell proliferation, arrest the cell cycle and induce apoptosis in UMUC3 bladder cancer cells. Investigational New Drugs, 35(6), 671–681. https://doi.org/10.1007/s10637-017-0483-7

Liu, C. L., Zhao, D., Li, J. J., Liu, S., An, J. J., Wang, D., Hu, F. A., Qiu, C. Y., & Cui, M. H. (2022). Inhibition of glioblastoma progression by urolithin A in vitro and in vivo by regulating Sirt1-FOXO1 axis via ERK/AKT signaling pathways. Neoplasma, 69, 80–94. https://doi.org/10.4149/neo_2021_210623N834

NCCNNetwork. (2020). NCCN clinical practice guidelines in oncology (NCCN guidelines): Gastric cancer. Version 1.

Norden, E., & Heiss, E. H. (2019). Urolithin A gains in antiproliferative capacity by reducing the glycolytic potential via the p53/TIGAR axis in colon cancer cells. Carcinogenesis, 40(1), 93–101. https://doi.org/10.1093/carcin/bgy158

Russell, R. C., Yuan, H. X., & Guan, K. L. (2014). Autophagy regulation by nutrient signaling. Cell Research, 24(1), 42–57. https://doi.org/10.1038/cr.2013.166

Sharma, M., Li, L., Celver, J., Killian, C., Kovoor, A., & Seeram, N. P. (2010). Effects of fruit ellagitannin extracts, ellagic acid, and their colonic metabolite, urolithin A, on Wnt signaling. Journal of Agricultural and Food Chemistry, 58(7), 3965–3969. https://doi.org/10.1021/jf902857v

Sung, H., Ferlay, J., Siegel, R. L., Laversanne, M., Soerjomataram, I., Jemal, A., & Bray, F. (2021). Global cancer statistics 2020: GLOBOCAN estimates of incidence and mortality worldwide for 36 cancers in 185 countries. CA: A Cancer Journal for Clinicians, 71(3), 209–249. https://doi.org/10.3322/caac.21660

Tang, L., Mo, Y., Li, Y., Zhong, Y., He, S., Zhang, Y., Tang, Y., Fu, S., Wang, X., & Chen, A. (2017). Urolithin A alleviates myocardial ischemia/reperfusion injury via PI3K/Akt pathway. Biochemical and Biophysical Research Communications, 486(3), 774–780. https://doi.org/10.1016/j.bbrc.2017.03.119

Totiger, T. M., Srinivasan, S., Jala, V. R., Lamichhane, P., Dosch, A. R., Gaidarski, A. A., 3rd, Joshi, C., Rangappa, S., Castellanos, J., Vemula, P. K., Chen, X., Kwon, D., Kashikar, N., VanSaun, M., Merchant, N. B., & Nagathihalli, N. S. (2019). Urolithin A, a novel natural compound to target PI3K/AKT/mTOR pathway in pancreatic cancer. Molecular Cancer Therapeutics, 18(2), 301–311. https://doi.org/10.1158/1535-7163.Mct-18-0464

Tuohetaerbaike, B., Zhang, Y., Tian, Y., Zhang, N., Kang, J., Mao, X., Zhang, Y., & Li, X. (2020). Pancreas protective effects of urolithin A on type 2 diabetic mice induced by high fat and streptozotocin via regulating autophagy and AKT/mTOR signaling pathway. Journal of Ethnopharmacology, 250, 112479. https://doi.org/10.1016/j.jep.2019.112479

Velagapudi, R., Lepiarz, I., El-Bakoush, A., Katola, F. O., Bhatia, H., Fiebich, B. L., & Olajide, O. A. (2019). Induction of autophagy and activation of SIRT-1 deacetylation mechanisms mediate neuroprotection by the pomegranate metabolite urolithin A in BV2 microglia

and differentiated 3D human neural progenitor cells. *Molecular Nutrition & Food Research*, *63*(10), 1801237. https://doi.org/10.1002/mnfr.201801237

Wang, Y., Qiu, Z., Zhou, B., Liu, C., Ruan, J., Yan, Q., Liao, J., & Zhu, F. (2015). In vitro antiproliferative and antioxidant effects of urolithin A, the colonic metabolite of ellagic acid, on hepatocellular carcinomas HepG2 cells. *Toxicology In Vitro*, *29*(5), 1107–1115. https://doi.org/10.1016/j.tiv.2015.04.008

Yang, Z. J., Chee, C. E., Huang, S., & Sinicrope, F. A. (2011). The role of autophagy in cancer: Therapeutic implications. *Molecular Cancer Therapeutics*, *10*(9), 1533–1541. https://doi.org/10.1158/1535-7163.Mct-11-0047

Zhang, Y., Aisker, G., Dong, H., Halemahebai, G., Zhang, Y., & Tian, L. (2021). Urolithin A suppresses glucolipotoxicity-induced ER stress and TXNIP/NLRP3/IL-1beta inflammation signal in pancreatic beta cells by regulating AMPK and autophagy. *Phytomedicine*, *93*, 153741. https://doi.org/10.1016/j.phymed.2021.153741

Zhang, X., Liang, H., Li, Z., Xue, Y., Wang, Y., Zhou, Z., & Ji, J. (2021). Perioperative or postoperative adjuvant oxaliplatin with S-1 versus adjuvant oxaliplatin with capecitabine in patients with locally advanced gastric or gastro-oesophageal junction adenocarcinoma undergoing D2 gastrectomy (RESOLVE): An open-label, superiority and non-inferiority, phase 3 randomised controlled trial. *The Lancet Oncology*, *22*(8), 1081–1092. https://doi.org/10.1016/s1470-2045(21)00297-7

Zhang, Y., Zhang, Y., Halemahebai, G., Tian, L., Dong, H., & Aisker, G. (2021). Urolithin A, a pomegranate metabolite, protects pancreatic β cells from apoptosis by activating autophagy. *Journal of Ethnopharmacology*, *272*, 113628. https://doi.org/10.1016/j.jep.2020.113628

Zhou, B., Wang, J., Zheng, G., & Qiu, Z. (2016). Methylated urolithin A, the modified ellagitannin-derived metabolite, suppresses cell viability of DU145 human prostate cancer cells via targeting miR-21. *Food and Chemical Toxicology*, *97*, 375–384. https://doi.org/10.1016/j.fct.2016.10.005

SUPPORTING INFORMATION

Additional supporting information can be found online in the Supporting Information section at the end of this article.